

Magnetism and metal-insulator transitions in the Rashba-Hubbard model

Welberth Kennedy ^{1,*}, Sebastião dos Anjos Sousa-Júnior ², Natanael C. Costa ² and Raimundo R. dos Santos ²

¹*Departamento de Física, Universidade Federal do Piauí, 64049-550 Teresina, Piauí, Brazil*

²*Instituto de Física, Universidade Federal do Rio de Janeiro, 21941-972 Rio de Janeiro, Rio de Janeiro, Brazil*



(Received 17 May 2022; accepted 11 October 2022; published 21 October 2022)

The nature of a metal-insulator and magnetic transitions is still a subject under intense debate in condensed-matter physics. Among the many possible mechanisms, the interplay between electronic correlations and spin-orbit couplings is an issue of a great deal of interest, in particular, when dealing with quasi-two-dimensional compounds. In view of this, here we use a Hartree-Fock approach to investigate how the Rashba spin-orbit coupling V_{SO} affects the magnetic ordering provided by a Hubbard interaction U on a square lattice. At half-filling, we have found a sequence of transitions for increasing V_{SO} : from a Mott insulator to a metallic antiferromagnet and then to a paramagnetic Rashba metal. Also, our results indicate that the Rashba coupling favors magnetic striped phases in the doped regime. By analyzing spectral properties, we associate the rearrangement of the magnetic ordering with the emerging chirality created by the spin-orbit coupling. Our findings provide insights towards clarifying the competition between these tendencies.

DOI: [10.1103/PhysRevB.106.165121](https://doi.org/10.1103/PhysRevB.106.165121)

I. INTRODUCTION

The interplay between strong electron correlations and spin-orbit coupling (SOC) has attracted a great deal of attention over recent years [1–4]. Theoretical interest has found echo in experimental studies both in materials, such as semiconductor heterostructures [5], carbon-based materials, pyrochlore iridates [4], and superconducting cuprates [6] as well as in ultracold fermionic atoms in optical lattices [7,8]. One of the reasons for such activity stems from the fact that the paradigmatic Mott insulating phase is affected by the presence of a SOC in a variety of ways, giving rise to many exotic quantum states of matter, such as topological insulators, Weyl semimetals, Kitaev spin liquids, and so forth [1–4]. SOC has also been predicted to modify more conventional ordered phases, such as magnetism and superconductivity as well as enhancing the possibility of superconducting triplet pairing [9].

Despite the intense activity, there is still no consensus on the mechanisms through which increasing SOC suppresses antiferromagnetic (AFM) order (or any spiral ordering) on the way to the above-mentioned more exotic phases. Indeed, even in the simplest case, namely, that of the single-band Hubbard model, the effects of Rashba SOC [10] on the ground-state phase diagram Un (where U is the on-site repulsion, and n is the band filling) are crucially dependent on the theoretical approach. At half-filling, a cluster dynamical mean-field theory predicts the existence of a metallic phase which eventually becomes an insulating phase as U increases with magnetic arrangements changing with the strength of the SOC [11]. Also at half-filling, a cluster perturbation theory recently found that the SOC favors the formation of a metallic state [12].

In view of this, we feel that a thorough examination of the ground-state phase diagram of the Hubbard model with

Rashba SOC is still lacking especially in the doped case. With this in mind, here we use a Hartree-Fock (HF) approach capable of detecting a diversity of spiral magnetic structures, while also shedding light on the metallic or insulating character of the phases involved. The layout of the paper is as follows. In Sec. II we present both the model and the highlights of the HF approach, whose results are presented and discussed in Sec. III. Conclusions are presented in Sec. IV.

II. MODEL AND METHODS

The system is described by the Hamiltonian,

$$\mathcal{H} = \mathcal{H}_H + \mathcal{H}_{\text{SO}}, \quad (1)$$

where

$$\mathcal{H}_H = -t \sum_{\langle \mathbf{i}, \mathbf{j} \rangle, \sigma} (c_{\mathbf{i}, \sigma}^\dagger c_{\mathbf{j}, \sigma} + \text{H.c.}) + U \sum_{\mathbf{i}} n_{\mathbf{i}\uparrow} n_{\mathbf{i}\downarrow} \quad (2)$$

is the usual Hubbard Hamiltonian describing fermions hopping (t is the hopping integral) between nearest-neighbor sites $\langle \mathbf{i}, \mathbf{j} \rangle$, of a square lattice $c_{\mathbf{i}\sigma}^\dagger$ ($c_{\mathbf{j}\sigma}$) creates (annihilates) a fermion with spin σ at site \mathbf{i} (\mathbf{j}), U is the strength of the on-site Coulomb repulsion, and $n_{\mathbf{i}\sigma} \equiv c_{\mathbf{i}\sigma}^\dagger c_{\mathbf{i}\sigma}$,

$$\mathcal{H}_{\text{SO}} = V_{\text{SO}} \sum_{\mathbf{i}, \sigma, \sigma'} [i(c_{\mathbf{i}, \sigma}^\dagger \sigma_{\sigma\sigma'}^x c_{\mathbf{i}+\hat{y}, \sigma'} - c_{\mathbf{i}, \sigma}^\dagger \sigma_{\sigma\sigma'}^y c_{\mathbf{i}+\hat{x}, \sigma'}) + \text{H.c.}] \quad (3)$$

describes the Rashba-type spin-orbit coupling, where V_{SO} is the strength of the Rashba SOC, and $\sigma_{\sigma\sigma'}^\tau$ is the σ, σ' ($=\uparrow, \downarrow$) element of the Pauli matrices $\hat{\sigma}^\tau$, $\tau = x, y$; H.c. stands for “Hermitian conjugate of the previous expression.” We note that \mathcal{H}_{SO} is written in the form of a kinetic term, which means that the *local* Rashba contribution is neglected. The reason for this lies in the fact that here we are primarily concerned in highlighting the effects arising from the breakdown of spatial

*welberthkennedy@icloud.com

inversion symmetry, which is preserved by the local Rashba SOC [13].

We probe the magnetic properties of the model within a Hartree-Fock approximation [14], which allows us to decouple the quartic terms of the Hamiltonian, leading to a quadratic form with the cost of adding effective Weiss fields with respect to which minimization will be sought; see below. In order to investigate the possibility of stabilizing spiral magnetic phases, we let the magnetization vector be defined as [14–17]

$$\mathbf{m}_i = \langle \mathbf{S}_i \rangle = m[\cos(\mathbf{Q} \cdot \mathbf{i}), \sin(\mathbf{Q} \cdot \mathbf{i}), 0], \quad (4)$$

with

$$\mathbf{S}_i = \frac{1}{2} \sum_{\sigma, \sigma' = \pm} c_{i, \sigma}^\dagger \boldsymbol{\sigma}_{\sigma \sigma'} c_{i, \sigma'}, \quad (5)$$

where $\boldsymbol{\sigma}$ is the vector operator whose components are the Pauli matrices and the magnetic wave-vector $\mathbf{Q} \equiv (q_x, q_y)$ characterizes the spiral phases. Within our scheme, both wave vector and magnetization amplitude m are determined self-consistently.

The Hartree-Fock Hamiltonian then becomes

$$\begin{aligned} \mathcal{H}_{\text{HF}} = & -t \sum_{(i,j), \sigma} (c_{i, \sigma}^\dagger c_{j, \sigma} + c_{j, \sigma}^\dagger c_{i, \sigma}) \\ & + V_{\text{SO}} \sum_{i, \sigma, \sigma'} [i(c_{i, \sigma}^\dagger \sigma_{\sigma \sigma'}^x c_{i+\hat{y}, \sigma'} - c_{i, \sigma}^\dagger \sigma_{\sigma \sigma'}^y c_{i+\hat{x}, \sigma'}) + \text{H.c.}] \\ & + U \sum_i \left[\frac{n}{2} n_i - 2\mathbf{m}_i \cdot \mathbf{S}_i - \frac{n^2}{4} + m^2 \right], \end{aligned} \quad (6)$$

where n is the the average electronic density. The diagonalization of \mathcal{H}_{HF} is more readily worked out in reciprocal space. Upon Fourier transforming Eq. (6), we obtain

$$\begin{aligned} \mathcal{H}_{\text{HF}} = & \sum_{\mathbf{k}} \left(\varepsilon_{\mathbf{k}} c_{\mathbf{k}\uparrow}^\dagger c_{\mathbf{k}\uparrow} + \varepsilon_{\mathbf{k}+\mathbf{q}} c_{\mathbf{k}+\mathbf{q}\uparrow}^\dagger c_{\mathbf{k}+\mathbf{q}\uparrow} + \frac{1}{2} n U n_{\mathbf{k}} \right) \\ & - U m \sum_{\mathbf{k}} (c_{\mathbf{k}\uparrow}^\dagger c_{\mathbf{k}+\mathbf{q}\downarrow} + c_{\mathbf{k}+\mathbf{q}\downarrow}^\dagger c_{\mathbf{k}\uparrow}) \\ & + \sum_{\mathbf{k}, \sigma, \sigma'} (\hat{V}_{\mathbf{k}})_{\sigma \sigma'} c_{\mathbf{k}\sigma}^\dagger c_{\mathbf{k}\sigma'}, \end{aligned} \quad (7)$$

where

$$\hat{V}_{\mathbf{k}} \equiv 2V_{\text{SO}}(\sigma^x \sin k_y - \sigma^y \sin k_x), \quad (8)$$

and the dispersion relation is $\varepsilon_{\mathbf{k}} = -2t(\cos k_x + \cos k_y)$. In what follows, we perform our analyses on lattices of 200×200 sites, which are large enough to disregard finite-size effects.

A. The noninteracting limit

If we set $U = 0$, the original Hamiltonian can be diagonalized by Fourier transforming into \mathbf{k} space, leading to the bands,

$$E_{\mathbf{k}}^\pm = \varepsilon_{\mathbf{k}} \pm 2V_{\text{SO}} \sqrt{\sin^2 k_x + \sin^2 k_y}, \quad (9)$$

and its correspondents eigenvectors,

$$|\pm, \mathbf{k}\rangle = \frac{1}{\sqrt{2}} \begin{pmatrix} 1 \\ \pm e^{-i\phi} \end{pmatrix}, \quad (10)$$

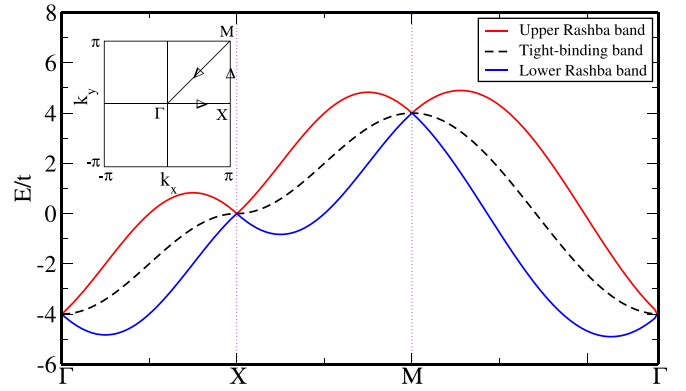


FIG. 1. Band structure along a path in \mathbf{k} space across the high-symmetry points of the square lattice (see the inset). The black dashed curve is $\varepsilon_{\mathbf{k}}$, the tight-binding band in the absence of the Rashba SOC, whereas the upper (red) and lower (blue) solid lines are the Rashba bands for $V_{\text{SO}}/t = 1$, and are labeled by $\alpha = \pm$, respectively.

in the spinor basis $\Psi_{\mathbf{k}} = (c_{\mathbf{k}\uparrow}^\dagger, c_{\mathbf{k}\downarrow}^\dagger)$ with $\tan \phi = \sin k_y / \sin k_x$. Figure 1 shows the splitting of the tight-binding band $\varepsilon_{\mathbf{k}}$, caused by the Rashba SOC: the lack of spatial inversion symmetry breaks the spin degeneracy in the conventional dispersion relation, thus, giving rise to two bands. Accordingly, these single-particle bands, each of which is labeled by a “chirality,” $\alpha = \pm$, describe a “Rashba metal” (RM); that is, the spin texture acquires a momentum dependence.

Examples of the noninteracting density of states (DOS) with Rashba SOC may be found in Refs. [18–20] from which we see that the van Hove singularity (vHS) present at the Fermi energy, ε_F at half-filling is split in two, symmetrically distributed around ε_F ; also, the nesting of the Fermi surface at half-filling is suppressed.

B. The interacting case

Introducing Nambu spinors,

$$\Phi_{\mathbf{k}} = (c_{\mathbf{k}\uparrow}^\dagger, c_{\mathbf{k}\downarrow}^\dagger, c_{\mathbf{k}+\mathbf{q}\uparrow}^\dagger, c_{\mathbf{k}+\mathbf{q}\downarrow}^\dagger), \quad (11)$$

the Hartree-Fock Hamiltonian Eq. (7) becomes

$$\mathcal{H}_{\text{HF}} = \frac{1}{2} \sum_{\mathbf{k}} \Phi_{\mathbf{k}} \hat{H}_{\mathbf{k}} \Phi_{\mathbf{k}}^\dagger + \sum_{\mathbf{k}} \left(\mu n + U m^2 - \frac{1}{4} U n^2 \right), \quad (12)$$

where

$$\hat{H}_{\mathbf{k}} = \begin{pmatrix} \bar{E}_{\mathbf{k}} & (\hat{V}_{\mathbf{k}})_{\uparrow\downarrow} & 0 & -Um \\ (\hat{V}_{\mathbf{k}})_{\downarrow\uparrow} & \bar{E}_{\mathbf{k}} & -Um & 0 \\ 0 & -Um & \bar{E}_{\mathbf{k}+\mathbf{q}} & (\hat{V}_{\mathbf{k}+\mathbf{q}})_{\uparrow\downarrow} \\ -Um & 0 & (\hat{V}_{\mathbf{k}+\mathbf{q}})_{\downarrow\uparrow} & \bar{E}_{\mathbf{k}+\mathbf{q}} \end{pmatrix}, \quad (13)$$

with

$$\bar{E}_{\mathbf{k}} = \varepsilon_{\mathbf{k}} - \mu + \frac{1}{2} U n, \quad (14)$$

and $(\hat{V}_{\mathbf{k}})_{\sigma \sigma'}$ are the spin-orbit matrix elements [see Eq. (8)]. With the HF Hamiltonian, Eq. (12), one solves a Schrödinger equation for a given \mathbf{k} , namely,

$$\hat{H}_{\mathbf{k}} |\psi_{\mathbf{k}}^v\rangle = \lambda_{\mathbf{k}}^{(v)} |\psi_{\mathbf{k}}^v\rangle, \quad (15)$$

from which we extract the eigenstates $|\psi_{\mathbf{k}}^{(\nu)}\rangle$ and their corresponding eigenvalues $\lambda_{\mathbf{k}}^{(\nu)}$ with ν being an integer labeling the quasiparticle bands. Therefore, the Helmholtz free energy may, therefore, be written as

$$F = -\frac{1}{\beta} \sum_{\mathbf{k}, \nu} \ln [1 + e^{-\beta \lambda_{\mathbf{k}}^{(\nu)}}] + \mu n - U \left(\frac{n^2}{4} - m^2 \right), \quad (16)$$

where $\beta = 1/k_B T$.

The fields m , $\mathbf{Q} = (q_x, q_y)$, and μ are determined self-consistently through the minimization of the Helmholtz free energy,

$$\left\langle \frac{\partial F}{\partial \mu} \right\rangle = \left\langle \frac{\partial F}{\partial m} \right\rangle = \left\langle \frac{\partial F}{\partial q_x} \right\rangle = \left\langle \frac{\partial F}{\partial q_y} \right\rangle = 0, \quad (17)$$

where one should not discard the possibility of having $q_x \neq q_y$. At this point, it is worth making a technical remark. Even though we are ultimately interested in the ground-state properties of the model, it turned out that the gain in convergence steps to find the minima is significant if we perform the minimization process at very low temperatures (hence, through the free energy) instead of the total (internal) energy. The errors involved by working at very low, but finite temperatures are indeed small; for instance, at a temperature $T \sim 1 \times 10^{-4}$ (in units of t/k_B), the difference between the free energy and the ground-state energy is smaller than 10^{-6} (in units of t).

Having in mind that several magnetic arrangements may occur, here we adopt the following strategy to determine the ground state. For fixed values of U/t , V_{SO} , and band filling n , we calculate the free energy assuming different magnetic wave vectors, $\mathbf{Q} = (q_x, q_y)$. For instance, the antiferromagnetic state corresponds to $m \neq 0$ and $q_x = q_y = \pi$, the ferromagnetic (FM) state to $m \neq 0$ and $q_x = q_y = 0$, and the paramagnetic state to $m = 0$. We also allow for other phases with $m \neq 0$, such as striped phases with $\mathbf{Q} = (q, 0)$ [and its symmetric $\mathbf{Q} = (0, q)$], or $\mathbf{Q} = (q, \pi)$ [$\mathbf{Q} = (\pi, q)$], as well as general spiral phases, $\mathbf{Q} = (q, q)$. With all the possible lowest free energies at hand, the ground state for the chosen values of U , V_{SO} , and n corresponds to the minimum free energy; the values of q are also varied, and checked whether changes increase or decrease the free energy. We then repeat for several other values of the control variables to set up the phase diagrams. In the next section, we present and discuss the results of this minimization for different values of the electronic density and interaction strengths; we have found it instructive to separate the discussion into undoped and doped cases.

III. RESULTS AND DISCUSSIONS

A. Half-filling

In the absence of the Rashba SOC, the ground state of the Hubbard model at half-filling is antiferromagnetic for any $U > 0$, as predicted both by the present HF approximation [14,21] and by determinant quantum Monte Carlo (DQMC) simulations [22]. Furthermore, the magnetization amplitude m increases with U as a result of the higher degree of fermion localization; this behavior is indeed verified within our approach when we follow the values of m with U for $V_{SO} = 0$ in Fig. 2. Actually, as a combined result of

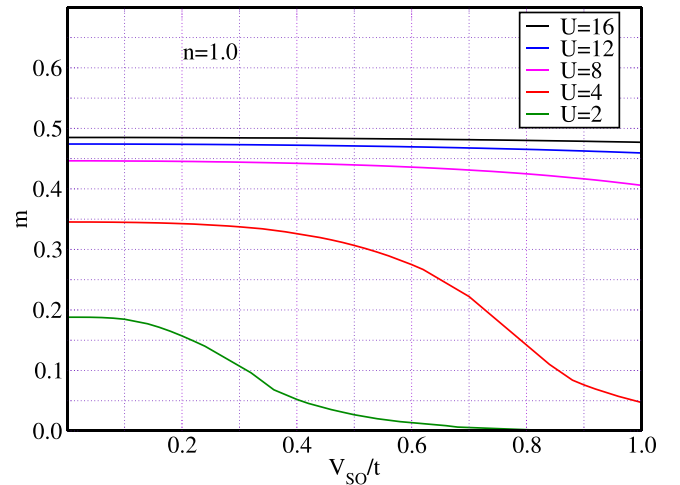


FIG. 2. Magnetization amplitude as a function of the spin-orbit coupling strength V_{SO} , at half-filling, and for different values of U/t , which decrease from the top curve to the bottom one.

the van Hove singularity and nesting at half-filling, $m \sim (t/U) \exp[-2\pi\sqrt{t/U}]$ within a HF approximation [22] in the weak-coupling regime.

When $V_{SO} \neq 0$, spin-flip processes come into play, which tend to disrupt the antiferromagnetically ordered state; this effect should be more effective at smaller on-site couplings. Indeed, Fig. 2 shows that the magnetization amplitude m decreases faster with V_{SO} for the smaller strengths of the Coulomb repulsion, and that for $U/t \gtrsim 8$ the SOC hardly affects the antiferromagnetic ordering within the physically appealing range of values $V_{SO}/t \lesssim 1$.

Figure 2 also shows that the magnetization amplitude m approaches zero very slowly with V_{SO} . Let us then take a closer look at the results for $U/t = 2$ for which the behavior of m with V_{SO}/t is shown again in Fig. 3, but now as a logarithmic-linear plot. As mentioned before (in the context of $U = 0$), the presence of a Rashba SOC splits the vHS into two peaks; Fig. 4 shows that this feature still occurs when $U/t = 2$ if $V_{SO} \lesssim 0.5$ and that it is located very close to the Fermi energy. We may, therefore, attribute this exponential decay of m to the influence of the nearby vHS-like peak. As seen for the periodic Anderson model [23], one expects that the mV_{SO} curves actually sharpen and acquire the usual order parameter behavior as the lattice size increases, or, equivalently, if the grid used in \mathbf{k} space gets denser. Instead of pursuing an investigation along these lines, for our purposes here it suffices to accept as the critical value $V_{SO,c}$ the value which renders $m/m_0 \lesssim \varepsilon$, where $m_0 = 1/2$ ($\hbar \equiv 1$) is the saturation value for spin 1/2, and ε is a tolerance. This, in turn, must be balanced with the fact that we are minimizing the free energy at low but finite temperatures. Indeed, the inset of Fig. 3 shows the estimates of $V_{SO,c}/t$ as a function of temperature for both $\varepsilon = 10^{-3}$ and $\varepsilon = 10^{-4}$: we see that the choice $\varepsilon = 10^{-3}$ leads to a stable value of $V_{SO,c}/t \approx 0.9$ as the temperature is lowered, so we take this as our working tolerance.

A question which immediately arises is whether the suppression of the antiferromagnetic phase is accompanied by a transition to a metallic state. In order to investigate this issue,

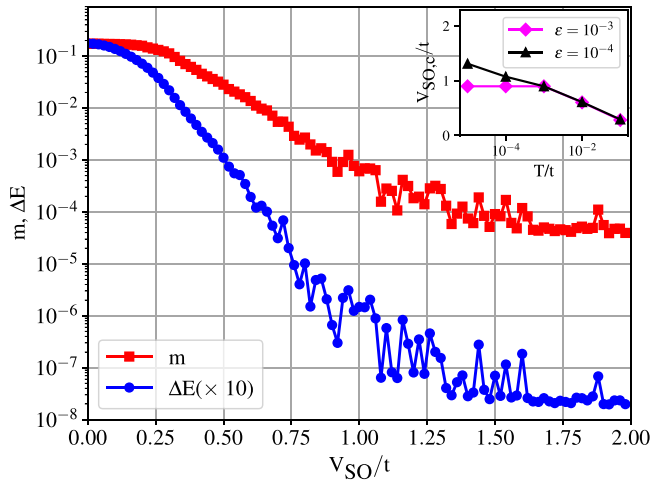


FIG. 3. Logarithm-linear plots for the magnetization amplitude, m (red squares), and the energy gap between antiferromagnetic and paramagnetic states, ΔE (blue circles) as functions of V_{SO} for $U/t = 2.0$ and $n = 1.0$. The inset shows the critical values of the Rashba SOC $V_{SO,c}$ for two fixed values of the “tolerance as zero” ε as functions of the temperature used in the minimization process [see Eq. (17)].

we examine the spectral properties. On one hand, we calculate the total (ground-state) energy assuming an AFM state as well as a RM state, and observe the gap ΔE between these energies as a function of V_{SO}/t for fixed U/t ; the outcome for $U/t = 2$ is shown in Fig. 3. One finds a decay towards zero faster than the one for m : more specifically, ΔE reaches a tolerance of $\tilde{\varepsilon}/t \sim 10^{-3}$ at $V_{SO,M}/t \approx 0.5$, which is almost half of $V_{SO,c}/t$ as determined from the behavior of m . We have also calculated the DOS on both sides of the transition; data for $U/t = 2$ are shown in Fig. 4. For small values of V_{SO} the behavior is reminiscent of what one would expect for a Mott insulator, namely, the van Hove singularity is split into two peaks separated by a gap around the Fermi energy. As V_{SO} increases, the gap narrows, forming a pseudogap near

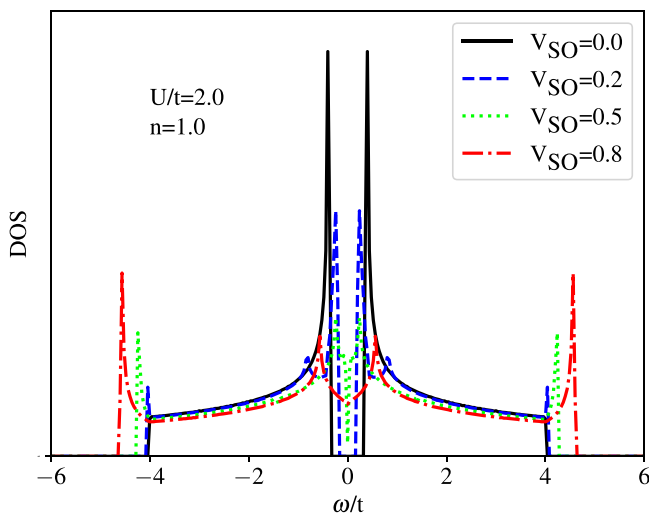


FIG. 4. Density of states at half-filling with $U/t = 2$, and different values of V_{SO}/t .

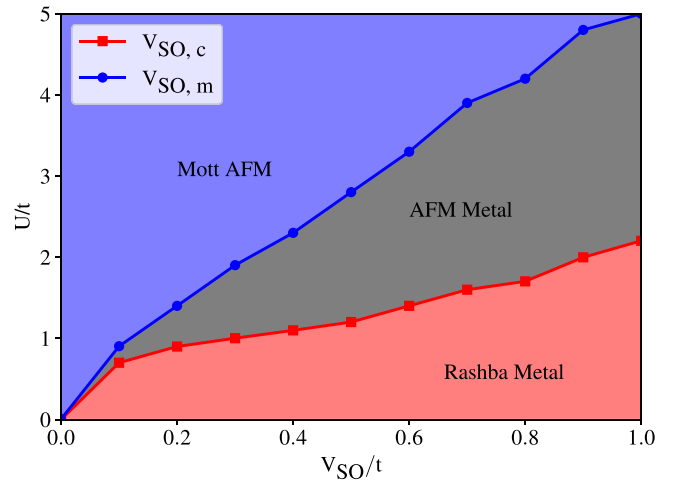


FIG. 5. Hartree-Fock phase diagram at half-filling. $V_{SO,c}$ denotes the critical curve for the transition between Rashba and antiferromagnetic metals, whereas $V_{SO,M}$ denotes the critical curve for the metal-insulator transition between antiferromagnetic states.

$V_{SO,M}/t \approx 0.5$; upon further increase in V_{SO} the gap closes leading to full metallic behavior. As a final test of our findings, we examined the possibility of the difference between the two critical points being caused by very shallow minima of the free energy but found that the minima are safely separated in V_{SO} . We, therefore, conclude that within our approach we have found a sequence of two transitions as V_{SO} increases, namely, first a Mott-AFM to an AFM metal, and then to a Rashba metal.

By employing the same procedure for different values of V_{SO} , we obtain the phase diagram shown in Fig. 5. We see that increasing V_{SO} at fixed U first drives the system from a Mott AFM phase to a metallic AFM phase; then, as U is further increased, the AFM gives way to a Rashba metallic phase. The fact that a Rashba SOC favors the appearance of a metallic phase is in line with the findings of Refs. [12,24] in which the strong V_{SO} regime was considered.

B. Doped regime

An early ground-state HF phase diagram, U vs doping $\delta \equiv 1 - n$ for the square lattice Hubbard model only involved the possibility of FM, AFM (Néel), and paramagnetic phases [22]; as generally expected for mean-field-like approaches, the outcome was qualitatively similar to the phase diagram obtained for the cubic lattice [25]. Later on, a HF approach allowing for spiral phases revealed that the Néel phase is indeed unstable against finite doping, giving way to incommensurate magnetic arrangements as well as to striped phases [14,21].

The suppression of antiferromagnetism for any doping is in agreement with predictions from DQMC simulations [22], thus, adding extra reliability to this approach. Indeed, this approach has revealed myriads of magnetic phases both in the Kondo-lattice model [15], and in a model [26] for coexistence of magnetism and superconductivity [16]; the latter work describes some features of the magnetic arrangements tuned by

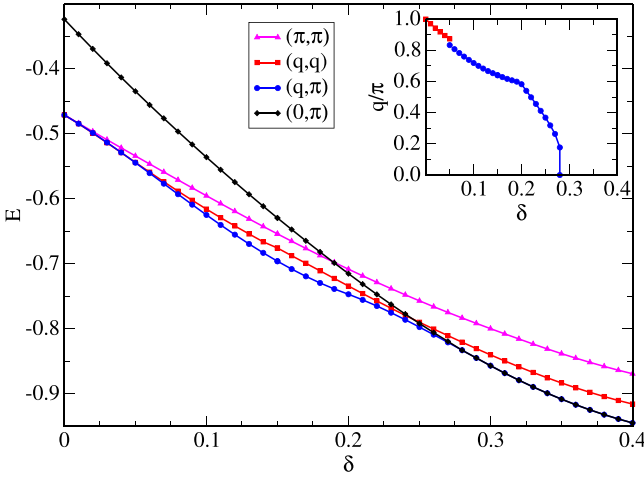


FIG. 6. Energy for different phases as a function of doping δ for fixed $V_{SO} = 0.5$ and $U/t = 9.0$. The inset shows the value of q/π as a function of doping for the striped phase (q, π) .

doping as experimentally observed in the borocarbide family of materials [27–29].

Away from half-filling, it is illustrative to compare the lowest energies, assuming different magnetic states, as functions of doping as shown in Fig. 6 for $V_{SO}/t = 0.5$ and $U/t = 9$. At very low doping, $\delta \lesssim 0.05$, the lowest-energy state corresponds to $\mathbf{Q} = (q, q)$, with q decreasing from π roughly linearly with δ (red squares in the inset of Fig. 6). In the interval $\delta \in [0.05, 0.3]$, the ground state corresponds to $\mathbf{Q} = (q, \pi)$ with q decreasing from 0.84 to 0 as shown in the inset of Fig. 6. At this doping the energy for $\mathbf{Q} = (q, \pi)$ (blue circles) joins smoothly with the one corresponding to $(0, \pi)$ (black diamonds). By repeating this procedure for other values of U and V_{SO} , we generate the phase diagrams displayed in Fig. 7.

Several features stand out when Fig. 7 is compared with the case $V_{SO} = 0$ [14,21,30]. First, for small doping the region of stability for the symmetric arrangement $\mathbf{Q} = (q, q)$ shrinks as V_{SO} increases, in favor of the striped phase $\mathbf{Q} = (q, \pi)$ [31]. Another noteworthy change is the fact that the phase $\mathbf{Q} = (0, q)$, located near $\delta = 0.7$, disappears with increasing V_{SO} so that one has a direct transition between a RM and a ferromagnet at large doping. By contrast, the size of the striped region $\mathbf{Q} = (0, \pi)$, centered around quarter-filling and with U/t around 9, is quite insensitive to the magnitude of the SOC.

From the above findings, we may conclude that, at least, for dopings up to quarter-filling, SOC tends to favor striped magnetic arrangements. Indeed, within a semiclassical picture the Rashba SOC favors the spins to point along directions perpendicular to the hopping direction, thus, a delicate balance with the Pauli principle is achieved by fermions flowing along the x and y lattice directions.

In order to understand the evolution of the magnetic wave vector with V_{SO} , we first define a spin chirality as [32]

$$\alpha(\mathbf{k}, \nu) = \langle \psi_{\mathbf{k}}^{\nu} | 2\mathbf{S} \cdot (\hat{\mathbf{k}} \times \hat{\mathbf{z}}) | \psi_{\mathbf{k}}^{\nu} \rangle, \quad (18)$$

where the $|\psi_{\mathbf{k}}^{\nu}\rangle$ are the HF ground states for $U \neq 0$; see Eq. (15). When $U \rightarrow 0$, $|\psi_{\mathbf{k}}^{\nu}\rangle \rightarrow |\pm, \mathbf{k}\rangle$ as given by Eq. (10) so that $\alpha(\mathbf{k}, \nu) \rightarrow \pm 1$; note, however, that for $U \neq 0$, $\alpha(\mathbf{k}, \nu)$

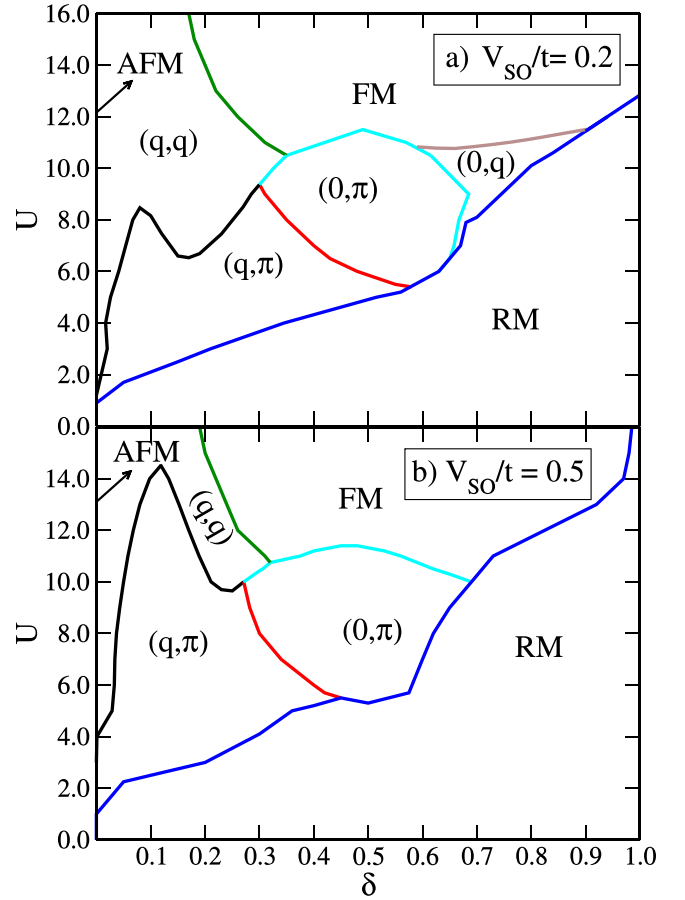


FIG. 7. Hartree-Fock phase diagrams U vs doping δ for (a) $V_{SO}/t = 0.2$, and (b) $V_{SO}/t = 0.5$. AFM stands for antiferromagnetic, FM stands for ferromagnetic, and RM stands for Rashba metal, whereas the spiral phases are labeled by $\mathbf{Q} \equiv (q_x, q_y)$; see the text. The black dashed lines separate the insulating phase, predominantly in the low-doping regime from the metallic phase in the high-doping regime.

may also vary continuously between ± 1 as we will see below. We now define projected spectral functions as follows:

$$A^{\pm}(\mathbf{k}, \omega) = \sum_{\nu} \alpha(\mathbf{k}, \nu) \delta(\omega - \lambda_{\mathbf{k}}^{(\nu)}), \quad (19)$$

so that the δ functions are weighted by the spin chirality, whose sign, in turn, labels the superscripts \pm in $A^{\pm}(\mathbf{k}, \omega)$. With $A^{\pm}(\mathbf{k}, \omega)$ at hand, we obtain the projected density of states as $D^{\pm}(\omega) = \sum_{\mathbf{k}} A^{\pm}(\mathbf{k}, \omega)$.

The top (bottom) row of Fig. 8 shows the DOS, D^{\pm} (spectral function A^{\pm}) for increasing intensities of the SOC. Note that for all values of V_{SO} , the DOS at the Fermi energy is finite, indicating metallic behavior as expected. For $V_{SO}/t = 0$, the bands are unsplit as they should, but nonzero values of V_{SO} cause a chirality splitting of the bands with dispersionless features around some points (notably around X) in the Brillouin zone being preserved. With increasing V_{SO} , the system becomes helically polarized, i.e., states below the Fermi level acquire a dominant $\alpha < 0$ character.

We are now in a position to examine the evolution of q [in $\mathbf{Q} = (q, \pi)$] with the SOC intensity. Figure 9 shows that for

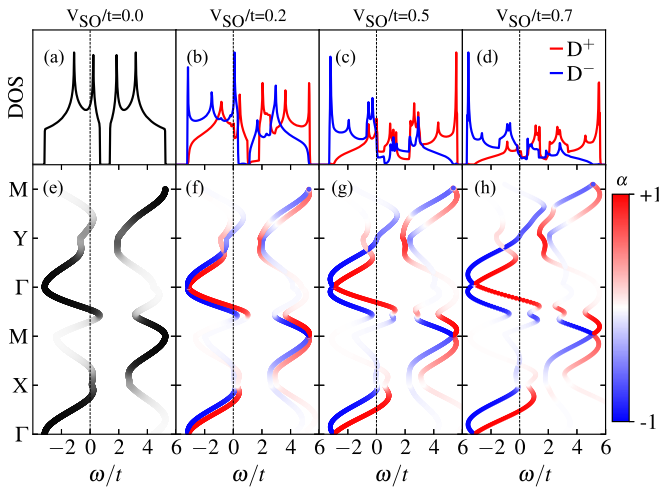


FIG. 8. Upper panel: Density of states for $n = 0.85$, $U/t = 5$, and (a) $V_{SO} = 0.0$, (b) 0.2 , (c) 0.5 , and (d) 0.7 . Lower panel: Projected spectral function for (e) $n = 0.85$, $U/t = 5$, and $V_{SO} = 0.0$, (f) 0.2 , (g) 0.5 , and (h) 0.7 ; the chirality α is indicated by the color map. In each case, the Fermi level is indicated by the dashed lines.

$U/t = 5$ and for both $n = 0.8$ and $n = 0.85$, q slowly changes with V_{SO} , until it reaches a peak and then steadily declines. Let us focus on Fig. 8, corresponding to filling $n = 0.85$. For $V_{SO}/t = 0.2$ the Fermi level lies at the vH singularity for D^- so that many states contribute to the averages; by contrast, beyond $V_{SO}/t = 0.5$, the contribution from the vH singularity is strongly suppressed, and q decreases. The inescapable conclusion is that the SOC strongly influences the magnetic ordering through changes in the spectral weight especially near the Fermi level. Alternatively, this may be viewed as a manifestation of the Rashba coupling renormalization by the electron-electron interaction [5,33], in particular, it has been recently established that the electron-electron interaction can also lead to nonlinearities in the Rashba coupling [34].

Finally, it is worth remarking that some aspects of the competition between Rashba and electron-electron interactions have been addressed in a continuum version [35], and their findings qualitatively agree with ours. Indeed, a comparison between our Figs. 5 and 7 with Fig. 1 of Ref. [35], shows that for small electron-electron interactions, nonmagnetic metallic phases are favored with the bands displaying a net chirality; we expect that our RM phase shares most of its properties with the chiral Fermi liquid phases of Ref. [35]. As the electron-electron interaction is increased, magnetically ordered phases dominate; while the *ansatz* we use here allows us to provide a detailed evolution of the wave-vector dependence of the magnetization (see below), we cannot distinguish between in-plane and out-of-plane polarizations as in Ref. [35].

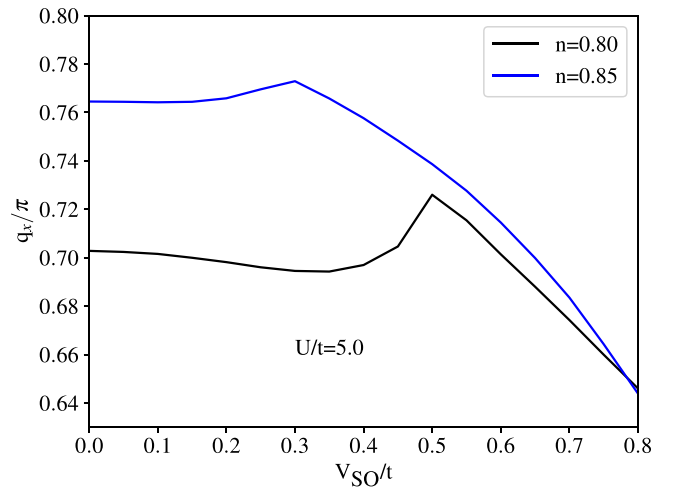


FIG. 9. The dependence of the wave vector with V_{SO} for $U/t = 5.0$.

IV. CONCLUSIONS

We have considered the Hubbard model in the presence of a Rashba SOC. Through a HF approach which allows for the presence of spiral magnetic arrangements, we have determined ground-state phase diagrams in the parameter space of on-site repulsion, U , SOC strength V_{SO} , and doping δ . At half-filling, we have established that for fixed U an increasing Rashba SOC drives a sequence of two transitions: from a Mott insulator to a metallic antiferromagnet and then to a paramagnetic Rashba metal. In the doped regime, several magnetic phases appear, including ferromagnetic and striped phases. Given that one has a very fine control of the repulsive interaction in ultracold atoms, we may envisage the possibility of generating a wide variety of magnetic arrangements simply by varying U and the doping level, say for fixed SOC; in the ultracold atoms scale, $V_{SO} \sim 0.5t$ corresponds to 30 nK, which is within reach of the lowest temperatures currently achieved [36–38]. One may also expect that the HF phase diagrams we have obtained here for a square lattice can serve as a guide to three-dimensional systems.

ACKNOWLEDGMENTS

We are grateful to the Brazilian Agencies Conselho Nacional de Desenvolvimento Científico e Tecnológico (CNPq), Coordenação de Aperfeiçoamento de Pessoal de Ensino Superior (CAPES), and Fundação Carlos Chagas de Apoio à Pesquisa do Estado do Rio de Janeiro (FAPERJ) for funding this project. N.C.C. acknowledges financial support from the Brazilian Agency CNPq, Grant No. 313065/2021-7.

- [1] W. Witczak-Krempa, G. Chen, Y. B. Kim, and L. Balents, Correlated quantum phenomena in the strong spin-orbit regime, *Annu. Rev. Condens. Matter Phys.* **5**, 57 (2014).
 [2] D. Bercioux and P. Lucignano, Quantum transport in Rashba spin-orbit materials: A review, *Rep. Prog. Phys.* **78**, 106001 (2015).

- [3] A. Manchon, H. C. Koo, J. Nitta, S. M. Frolov, and R. A. Duine, New perspectives for Rashba spin-orbit coupling, *Nature Mater.* **14**, 871 (2015).
 [4] J. Bertinshaw, Y. K. Kim, G. Khaliullin, and B. J. Kim, Square lattice iridates, *Annu. Rev. Condens. Matter Phys.* **10**, 315 (2019).

- [5] D. Maryenko, M. Kawamura, A. Ernst, V. K. Dugaev, E. Ya. Sherman, M. Kriener, M. S. Bahramy, Y. Kozuka, and M. Kawasaki, Interplay of spin-orbit coupling and Coulomb interaction in ZnO-based electron system, *Nat. Commun.* **12**, 3180 (2021).
- [6] K. Gotlieb, C.-Y. Lin, M. Serbyn, W. Zhang, C. L. Smallwood, C. Jozwiak, H. Eisaki, Z. Hussain, A. Vishwanath, and A. Lanzara, Revealing hidden spin-momentum locking in a high-temperature cuprate superconductor, *Science* **362**, 1271 (2018).
- [7] S. Kolkowitz, S. L. Bromley, T. Bothwell, M. L. Wall, G. E. Marti, A. P. Koller, X. Zhang, A. M. Rey, and J. Ye, Spin-orbit-coupled fermions in an optical lattice clock, *Nature (London)* **542**, 66 (2017).
- [8] B. Song, C. He, S. Niu, L. Zhang, Z. Ren, X.-J. Liu, and G.-B. Jo, Observation of nodal-line semimetal with ultracold fermions in an optical lattice, *Nat. Phys.* **15**, 911 (2019).
- [9] A. Greco and A. P. Schnyder, Mechanism for Unconventional Superconductivity in the Hole-Doped Rashba-Hubbard Model, *Phys. Rev. Lett.* **120**, 177002 (2018).
- [10] E. Rashba, Properties of semiconductors with an extremum loop. 1. cyclotron and combinational resonance in a magnetic field perpendicular to the plane of the loop, *Sov. Phys.-Solid State* **2**, 1109 (1960).
- [11] X. Zhang, W. Wu, G. Li, L. Wen, Q. Sun, and A.-C. Ji, Phase diagram of interacting Fermi gas in spin-orbit coupled square lattices, *New J. Phys.* **17**, 073036 (2015).
- [12] V. Brosco and M. Capone, Rashba-metal to Mott-insulator transition, *Phys. Rev. B* **101**, 235149 (2020).
- [13] T. Mii, N. Shima, K. Kano, and K. Makoshi, Spin-orbit interaction in the tight-binding model—toward the comprehension of the Rashba effect at surfaces, *J. Phys. Soc. Jpn.* **83**, 064706 (2014).
- [14] M. Dzierzawa, Hartree-Fock theory of spiral magnetic order in the 2-d Hubbard model, *Z. Phys. B: Condens. Matter* **86**, 49 (1992).
- [15] N. C. Costa, J. Pimentel de Lima, and R. R. dos Santos, Spiral magnetic phases on the Kondo lattice model: A Hartree-Fock approach, *J. Magn. Magn. Mater.* **423**, 74 (2017).
- [16] N. C. Costa, J. Pimentel de Lima, T. Paiva, M. El Massalami, and R. R. dos Santos, A mean-field approach to Kondo-attractive-Hubbard model, *J. Phys.: Condens. Matter* **30**, 045602 (2018).
- [17] S. dos Anjos Sousa-Júnior, J. P. de Lima, N. C. Costa, and R. R. dos Santos, Superconducting Kondo phase in an orbitally separated bilayer, *Phys. Rev. Res.* **2**, 033168 (2020).
- [18] Z. Li, L. Covaci, M. Berciu, D. Baillie, and F. Marsiglio, Impact of spin-orbit coupling on the Holstein polaron, *Phys. Rev. B* **83**, 195104 (2011).
- [19] A. Ptok, K. Rodríguez, and K. J. Kapcia, Superconducting monolayer deposited on substrate: Effects of the spin-orbit coupling induced by proximity effects, *Phys. Rev. Mater.* **2**, 024801 (2018).
- [20] J. Hutchinson, J. E. Hirsch, and F. Marsiglio, Enhancement of superconducting T_c due to the spin-orbit interaction, *Phys. Rev. B* **97**, 184513 (2018).
- [21] P. A. Igoshev, M. A. Timirgazin, V. F. Gilmudinov, A. K. Arzhnikov, and V. Yu. Irkhin, Spiral magnetism in the single-band Hubbard model: The Hartree-Fock and slave-boson approaches, *J. Phys.: Condens. Matter* **27**, 446002 (2015).
- [22] J. E. Hirsch, Two-dimensional Hubbard model: Numerical simulation study, *Phys. Rev. B* **31**, 4403 (1985).
- [23] W. Hu, R. T. Scalettar, E. W. Huang, and B. Moritz, Effects of an additional conduction band on the singlet-antiferromagnet competition in the periodic Anderson model, *Phys. Rev. B* **95**, 235122 (2017).
- [24] V. Brosco, D. Guerci, and M. Capone, Pauli metallic ground state in Hubbard clusters with Rashba spin-orbit coupling, *Phys. Rev. B* **97**, 125103 (2018).
- [25] D. R. Penn, Stability theory of the magnetic phases for a simple model of the transition metals, *Phys. Rev.* **142**, 350 (1966).
- [26] P. R. Bertussi, A. L. Malvezzi, T. Paiva, and R. R. dos Santos, Kondo-attractive-Hubbard model for the ordering of local magnetic moments in superconductors, *Phys. Rev. B* **79**, 220513(R) (2009).
- [27] M. ElMassalami, H. Takeya, B. Ouladdiaf, R. Maia Filho, A. M. Gomes, T. Paiva, and R. R. dos Santos, Tuning in magnetic modes in $\text{Tb}(\text{Co}_x \text{Ni}_{1-x})_2 \text{B}_2 \text{C}$: From longitudinal spin-density waves to simple ferromagnetism, *Phys. Rev. B* **85**, 174412 (2012).
- [28] M. ElMassalami, A. M. Gomes, T. Paiva, R. R. dos Santos, and H. Takeya, Evolution of magnetism in $\text{Tb}(\text{Co}_x \text{Ni}_{1-x})_2 \text{B}_2 \text{C}$, *J. Magn. Magn. Mater.* **335**, 163 (2013).
- [29] M. ElMassalami, H. Takeya, B. Ouladdiaf, A. M. Gomes, T. Paiva, and R. R. dos Santos, Evolution of magnetic layers stacking sequence within the magnetic structure of $\text{Ho}(\text{Co}_x \text{Ni}_{1-x})_2 \text{B}_2 \text{C}$, *J. Magn. Magn. Mater.* **372**, 74 (2014).
- [30] B.-G. Liu, Incommensurate antiferromagnetic orders and peculiar electronic structures in the doped Hubbard model, *J. Phys.: Condens. Matter* **6**, L415 (1994).
- [31] One should keep in mind that the exchange symmetry $q_x \leftrightarrow q_y$ applies, i.e., the solutions $\mathbf{q} = (q_x, q_y)$ and $\mathbf{q} = (q_y, q_x)$ are degenerate.
- [32] J.-H. Park, C. H. Kim, H.-W. Lee, and J. H. Han, Orbital chirality and Rashba interaction in magnetic bands, *Phys. Rev. B* **87**, 041301(R) (2013).
- [33] G.-H. Chen and M. E. Raikh, Exchange-induced enhancement of spin-orbit coupling in two-dimensional electronic systems, *Phys. Rev. B* **60**, 4826 (1999).
- [34] X. Yuan and P. S. Riseborough, Nonlinear Rashba effect in a strongly correlated system, *Europhys. Lett.* **139**, 46001 (2022).
- [35] W. E. Liu, S. Chesi, D. Webb, U. Zülicke, R. Winkler, R. Joynt, and D. Culcer, Generalized Stoner criterion and versatile spin ordering in two-dimensional spin-orbit coupled electron systems, *Phys. Rev. B* **96**, 235425 (2017).
- [36] I. Bloch, J. Dalibard, and W. Zwerger, Many-body physics with ultracold gases, *Rev. Mod. Phys.* **80**, 885 (2008).
- [37] T. Esslinger, Fermi-Hubbard physics with atoms in an optical lattice, *Annu. Rev. Condens. Matter Phys.* **1**, 129 (2010).
- [38] D. Mitra, P. T. Brown, E. Guardado-Sanchez, S. S. Kondov, T. Devakul, D. A. Huse, P. Schauss, and W. S. Bakr, Quantum gas microscopy of an attractive Fermi-Hubbard system, *Nat. Phys.* **14**, 173 (2018).